THE JOURNAL OF BIOLOGICAL CHEMISTRY VOL. 289, NO. 37, pp. 25611–25623, September 12, 2014

Dimeric Switch of Hakai-truncated Monomers during Substrate Recognition

*INSIGHTS FROM SOLUTION STUDIES AND NMR STRUCTURE**

Received for publication, June 28, 2014, and in revised form, July 21, 2014 Published, JBC Papers in Press, July 29, 2014, DOI 10.1074/jbc.M114.592840

Manjeet Mukherjee[‡1], **Fan Jing-Song**[‡], **Sarath Ramachandran**[‡], **Graeme R. Guy**[§], **and J. Sivaraman**[‡2]

From the [‡]*Department of Biological Sciences, 14 Science Drive 4, National University of Singapore, Singapore 117543 and the* [§]*Institute of Molecular and Cell Biology, 61 Biopolis Drive, Proteos, Singapore 138673*

Background: The novel phosphotyrosine-binding domain (HYB) of Hakai forms an atypical, zinc-coordinated homodimer.
Results: C-terminal truncation of the HYB domain causes dramatic structural changes and it becomes a monomer, but in the presence of substrate, it becomes a dimer to recognize the substrate.
Conclusion: HYB dimerization is a unique prerequisite for substrate-binding activity of Hakai.
Significance: The HYB domain may orchestrate the function of Hakai in cancer and cell-cell contacts.

Hakai, an E3 ubiquitin ligase, disrupts cell-cell contacts in epithelial cells and is up-regulated in human colon and gastric adenocarcinomas. Hakai acts through its phosphotyrosine-binding (HYB) domain, which bears a dimeric fold that recognizes the phosphotyrosine motifs of E-cadherin, cortactin, DOK1, and other Src substrates. Unlike the monomeric nature of the SH2 and phosphotyrosine-binding domains, the architecture of the HYB domain consists of an atypical, zinc-coordinated tight homodimer. Here, we report a C-terminal truncation mutant of the HYB domain ($HYB^{\Delta C}$), comprising amino acids 106–194, which exists as a monomer in solution. The NMR structure revealed that this deletion mutant undergoes a dramatic structural change caused by a rearrangement of the atypical zinc-coordinated unit in the C terminus of the HYB domain to a C_2H_2-like zinc finger in $HYB^{\Delta C}$. Moreover, using isothermal titration calorimetry, we show that dimerization of $HYB^{\Delta C}$ can be induced using a phosphotyrosine substrate peptide. This ligand-induced dimerization of $HYB^{\Delta C}$ is further validated using analytical ultracentrifugation, size-exclusion chromatography, NMR relaxation studies, dynamic light scattering, and circular dichroism experiments. Overall, these observations suggest that the dimeric architecture of the HYB domain is essential for the phosphotyrosine-binding property of Hakai.

Phosphotyrosine (Tyr(P))[3]-binding domains are key determinants of specificity and selectivity in many signal transduction pathways and act by integrating Tyr(P) signals from upstream kinases to downstream effectors that regulate the complex physiology of eukaryotic cells (1–3). The SH2 domain was the first Tyr(P)-binding domain to be discovered (4, 5) and has since been extensively characterized (1, 6–10). The second domain to be identified with a capacity to bind tyrosine residues was the phosphotyrosine-binding domain (11). Subsequently, idiosyncratic Tyr(P)-binding domains have been observed in the C2 domain of protein kinase Cδ (12) and pyruvate kinase M2 (13), and we recently reported the existence of a third Tyr(P)-binding domain in Hakai, coined the HYB domain for Hakai phosphotyrosine (Tyr(P)) binding (14).

Hakai is an E3-ubiquitin ligase first noted for its role in regulating E-cadherin expression and disrupting cell-cell contacts in epithelial tissues (15, 16). Subsequent work has identified the elevated expression of Hakai in human colon and gastric adenocarcinomas (17, 18). The HYB domain interacts with other Src substrates, such as Cortactin, a structural protein involved in coordinating actin rearrangement during cell movement (19), and DOK1, a scaffolding protein that assists in the assembly of signaling complexes (20). Both of these proteins offer important functional contributions in the progression of cancer (21, 22), and both are regulated by the activity of Hakai (14). The novel features of the HYB domain and its interaction with various key molecules may indicate a physiologically important role for Hakai in cancer.

The structure of the HYB domain was determined by x-ray crystallography (14). It comprises amino acids 106–206, and forms an atypical, zinc-coordinated homodimer in an antiparallel, intertwined configuration, utilizing residues from the Tyr(P)-binding region of two Hakai monomers. The dimeric nature of the domain configures the formation of a Tyr(P)-binding pocket that recognizes specific phosphorylated tyrosine residues and flanking acidic amino acids of its substrates (14). The C-terminal region, which harbors the atypical zinc-coordination motif and key residues involved in the Tyr(P) interaction, plays an important role in the dimerization observed in the HYB domain. In the present study, we investigated the consequences of deleting residues from the C terminus of Hakai, whereas maintaining the essential residues involved in the Tyr(P) interaction and the atypical zinc-coordi-

* This work was supported by MOE (Tier 2) Grant R154000625112.
The NMR data and structure of $HYB^{\Delta C}$ have been deposited in the Biological Magnetic Resonance Bank under accession number BMRB 25008.
The atomic coordinates and structure factors (code 2mq1) have been deposited in the Protein Data Bank (http://wwpdb.org/).
[1] Graduate scholar supported by the National University of Singapore.
[2] To whom correspondence should be addressed. E-mail: dbsjayar@nus.edu.sg.
[3] The abbreviations used are: Tyr(P), phosphotyrosine; aa, amino acid(s); BisTris, 2-[bis(2-hydroxyethyl)amino]-2-(hydroxymethyl)propane-1,3-diol; HYB, Hakai Tyr(P)-binding domain; RDC, residue dipolar coupling; AUC, analytical ultracentrifugation; HSQC, heteronuclear single quantum coherence; r.m.s., root mean square; ITC, isothermal titration calorimetry; PDB, Protein Data Bank; SH2, Src homology 2.

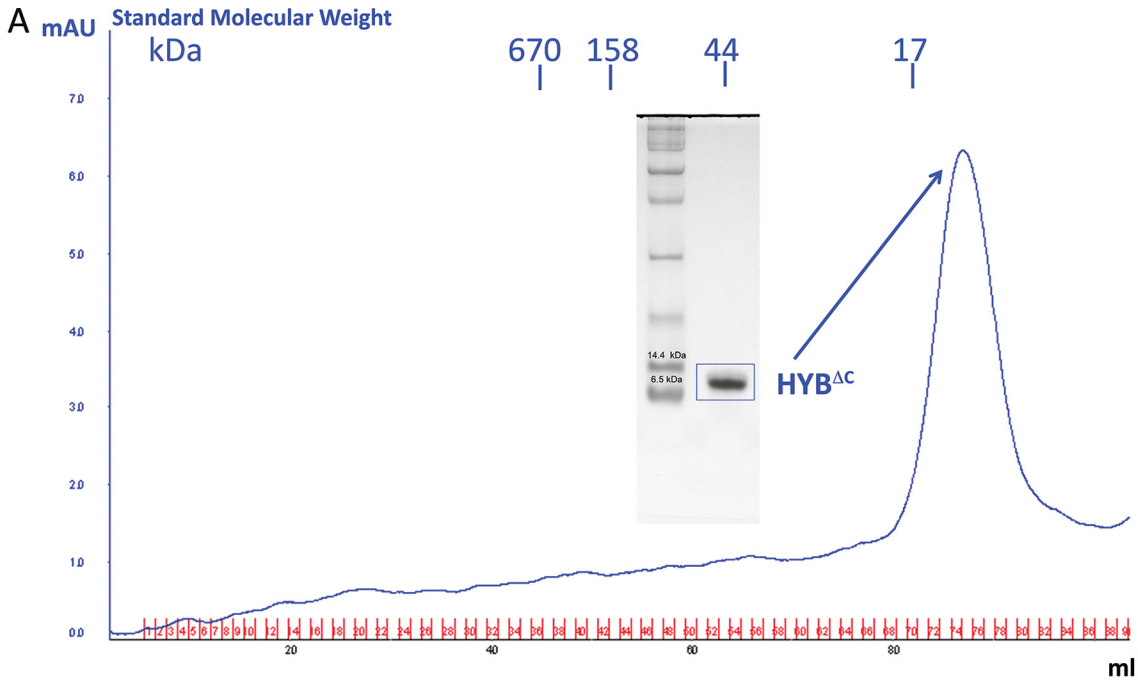
A
mAU
Standard Molecular Weight
kDa
670
158
44
17
14.4 kDa
6.5 kDa
HYB^ΔC
ml

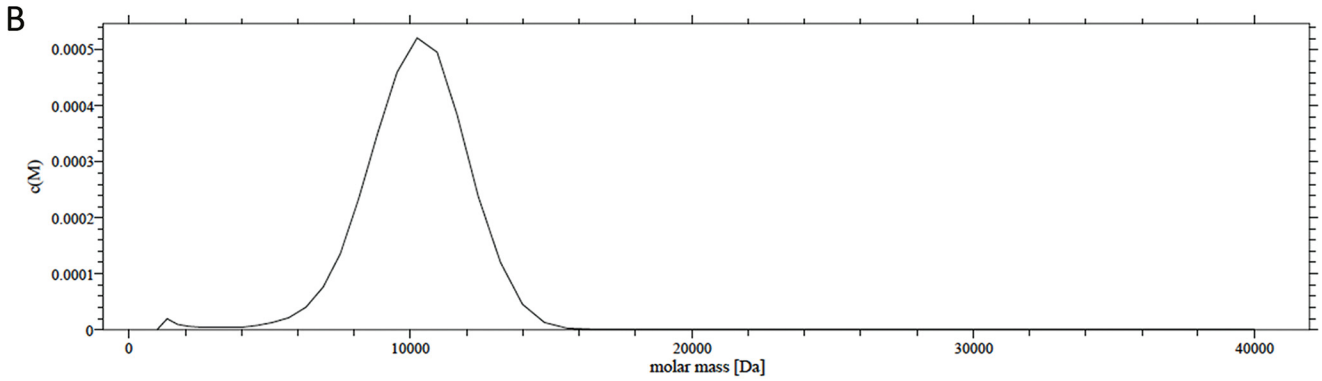
B
c(M)
molar mass [Da]

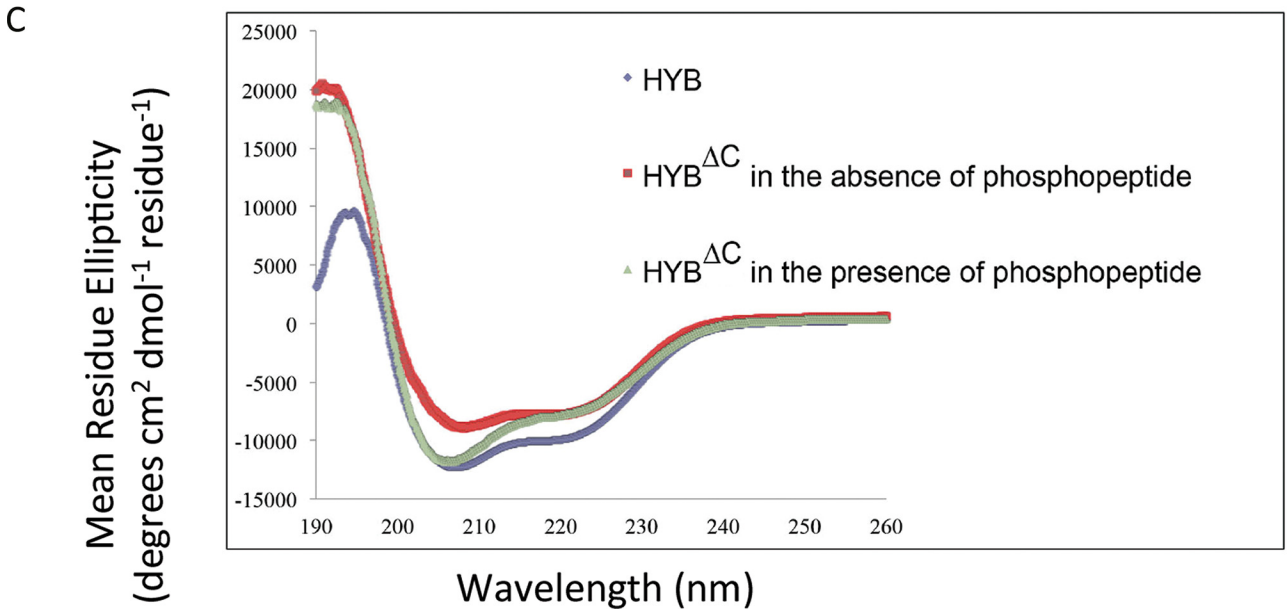
C
Mean Residue Ellipticity
(degrees cm² dmol⁻¹ residue⁻¹)
HYB
HYB^ΔC in the absence of phosphopeptide
HYB^ΔC in the presence of phosphopeptide
Wavelength (nm)

nation of the E3 ligase. Through this structural truncation, we identified a C-terminal deletion mutant of Hakai (aa 106–194), herein referred to as $HYB^{\Delta C}$, which exists as a monomer in solution and flips to a dimeric arrangement in the presence of a Tyr(P) substrate, with the incoming substrate inducing the conformational changes required to initiate dimerization of $HYB^{\Delta C}$ monomers. This monomeric to dimeric switch of $HYB^{\Delta C}$ in the presence of the phosphorylated substrate was further validated by biophysical studies. Taken together, our results suggest that the dimerization of Hakai Tyr(P)-binding domain is a unique prerequisite for substrate binding.

EXPERIMENTAL PROCEDURES

Protein Expression and Purification—Sequences corresponding to aa 106–194 of Hakai were cloned into pGEX6P-1 vector (GE Healthcare) using BamHI and SalI restriction sites, and expressed as a GST fusion protein in *Escherichia coli* BL21 (DE3) cells. Cells were cultured in LB medium at 37 °C until the $A_{600\,nm}$ reached 0.6–0.7. Cells were then incubated with 0.15 mM isopropyl 1-thio-β-D-galactopyranoside and 50 μM zinc sulfate, and then grown for an additional 20 h at 15 °C. Cells were collected by centrifugation (8000 × *g*, 10 min, 4 °C), and the pellets were resuspended in lysis buffer (50 mM BisTris, pH 6.5, 300 mM NaCl, 10 μM zinc chloride, 5% glycerol, 0.5% Triton X-100, 2 mM DTT, 1 mM phenylmethylsulfonyl fluoride) and homogenized using a French Press Cell Disrupter (Thermo Scientific, Wilmington, DE). Cell lysates were then centrifuged at 18,000 × *g* for 30 min at 4 °C (JA-25.50 fixed angle rotor centrifuge, Beckman Coulter, Fullerton, CA) and the supernatant was passed through glutathione-Sepharose resin (GE Healthcare) for 2–4 h at 4 °C. The resin was subsequently washed with a buffer containing 50 mM BisTris, pH 6.5, 300 mM NaCl, 5% glycerol, and 2 mM DTT, and the bound supernatant was then subjected to an overnight on-column cleavage at 4 °C with GST-PreScission Protease (GE Healthcare) to remove the GST tag. A major portion of GST and GST-PreScission Protease remained bound to the glutathione-Sepharose resin and the flow-through containing the partially purified, untagged proteins were further purified using a Superdex 75 size exclusion column (GE Healthcare) equilibrated with a buffer containing 50 mM sodium phosphate buffer, pH 6.5, and 5 mM DTT.

Circular Dichroism Spectrometry—Far UV spectra (260–190 nm) of HYB (aa 106–206) and $HYB^{\Delta C}$ (aa 106–194) in the absence and presence phosphorylated peptide of E-cadherin (residues 747–759) were measured using a Jasco J-810 spectropolarimeter in phosphate buffer, pH 6.5, at room temperature with a 0.1-cm path length and stoppered cuvettes. The protein concentration was maintained at 20 μM in all cases. Six scans were recorded, averaged, and the baseline subtracted. The scale on the CD spectra was normalized to mean residue ellipticity (MRE), which is measured in degrees cm^2 $dmol^{-1}$ $residue^{-1}$ using the following equation (23),

$$MRE = \theta \times (0.1 \times MRW)/(P \times CONC) \qquad \text{(Eq. 1)}$$

where θ is raw ellipticity measured in machine units (millidegrees), MRW is mean residue weight (MRW = protein mean weight (in daltons)/(number of residues) for the protein, *P* is path length in cm, and *CONC* is protein concentration in mg/ml. The MRE is plotted against the corresponding wavelength.

Dynamic Light Scattering—Dynamic light scattering studies were carried out on a DynaPro Light Scattering instrument (Wyatt Technology Europe GmbH, Dernbach, Germany) with protein concentrations at $A_{280\,nm}$ of 1.0, in buffer containing 50 mM sodium phosphate, pH 6.5, and 5 mM DTT.

NMR Spectroscopy—All NMR experiments were carried out at 25 °C on a Bruker Avance 800 MHz spectrometer equipped with a TXI cryogenic probe using 1 mM ^{13}C,^{15}N-labeled $HYB^{\Delta C}$

TABLE 1
NMR data and structure determination details for $HYB^{\Delta C}$

NMR data	
All NOE distance restraints[a]	1087
Intra-residue	224
Sequential ($\|i-j\| = 1$)	338
Medium range ($1 < \|i-j\| < 5$)	193
Long range ($\|i-j\| \geq 5$)	344
Hydrogen bond restraints	21
Dihedral angle restraints (φ, ψ)[b]	110
Residual dipolar coupling restraints	55
Energy statistics	
X-PLOR energy (kcal mol^{-1})	
E_{noe}	76.1 ± 4.8
E_{cdih}	1.26 ± 0.26
E_{rdc}	20.2 ± 3.7
Deviations from idealized covalent geometry[c]	
R.m.s. deviations of bond lengths (Å)	0.0031 ± 0.0031
R.m.s. deviations of bond angles (°)	0.430 ± 0.015
R.m.s. deviations of improper angles (°)	0.358 ± 0.011
Deviations from experimental restraints	
R.m.s. deviations of distance restraints (Å)	0.0369 ± 0.0012
R.m.s. deviations of dihedral angle restraints (°)	0.265 ± 0.074
Ramachandran plot analysis (%)[d]	
Residues in allowed region	96.9%
Residues in generally allowed regions	2.3%
Residues in disallowed regions	0.8%
Average R.m.s. deviations from mean structure (Å)[e]	
Heavy atoms	1.29 ± 0.21
Backbone atoms (N, CA, C′, O)	0.63 ± 0.21

[a] The distance restraints were obtained by classifying the NOE cross peaks into three categories: strong (1.8–2.9 Å), medium (1.8–3.5 Å), and weak (1.8–5.0 Å).
[b] Dihedral angles of backbone ϕ and ψ were predicted by TALOS (30) using the chemical shifts of Cα, Cβ, Hα, N, and HN.
[c] Twenty lowest-energy conformers with no NOE violations greater than 0.3 Å and no torsion angle violations greater than 3° were selected from 100 conformers to represent the NMR ensembles.
[d] Calculated with PROCHECK-NMR (66).
[e] Calculated with MOLMOL (67) over secondary structure region α1 (131–140), α2 (179–190), β1 (119–123), β2 (127–130) and β3 (154–158).

FIGURE 1. **Gel filtration, analytical ultracentrifugation, and circular dichroism of the $HYB^{\Delta C}$ (aa 106–194).** *A,* gel filtration profile of $HYB^{\Delta C}$. $HYB^{\Delta C}$ was loaded onto a calibrated Superdex-75 gel filtration chromatography column. The elution profile suggests that $HYB^{\Delta C}$ exists as a monomer. The SDS-PAGE analysis of $HYB^{\Delta C}$ depicts the purity and the molecular mass of the peak fraction (~10 kDa). *B,* AUC analysis of $HYB^{\Delta C}$. The monomeric nature of $HYB^{\Delta C}$ was studied using sedimentation velocity analysis. The molecular mass profile of $HYB^{\Delta C}$ indicates that the protein exists as a monomer in solution, with an apparent molecular mass of 10 kDa. *C,* circular dichroism analysis shows a significant difference in the secondary structure composition between $HYB^{\Delta C}$ and the untruncated HYB domain. Furthermore, in the presence of the phosphotyrosine peptide ligand (E-cadherin-(747–759)), the CD spectrum of $HYB^{\Delta C}$ shows marked resemblance with that of the HYB domain, suggesting a conformational change in $HYB^{\Delta C}$ in the presence of the phosphorylated ligand.

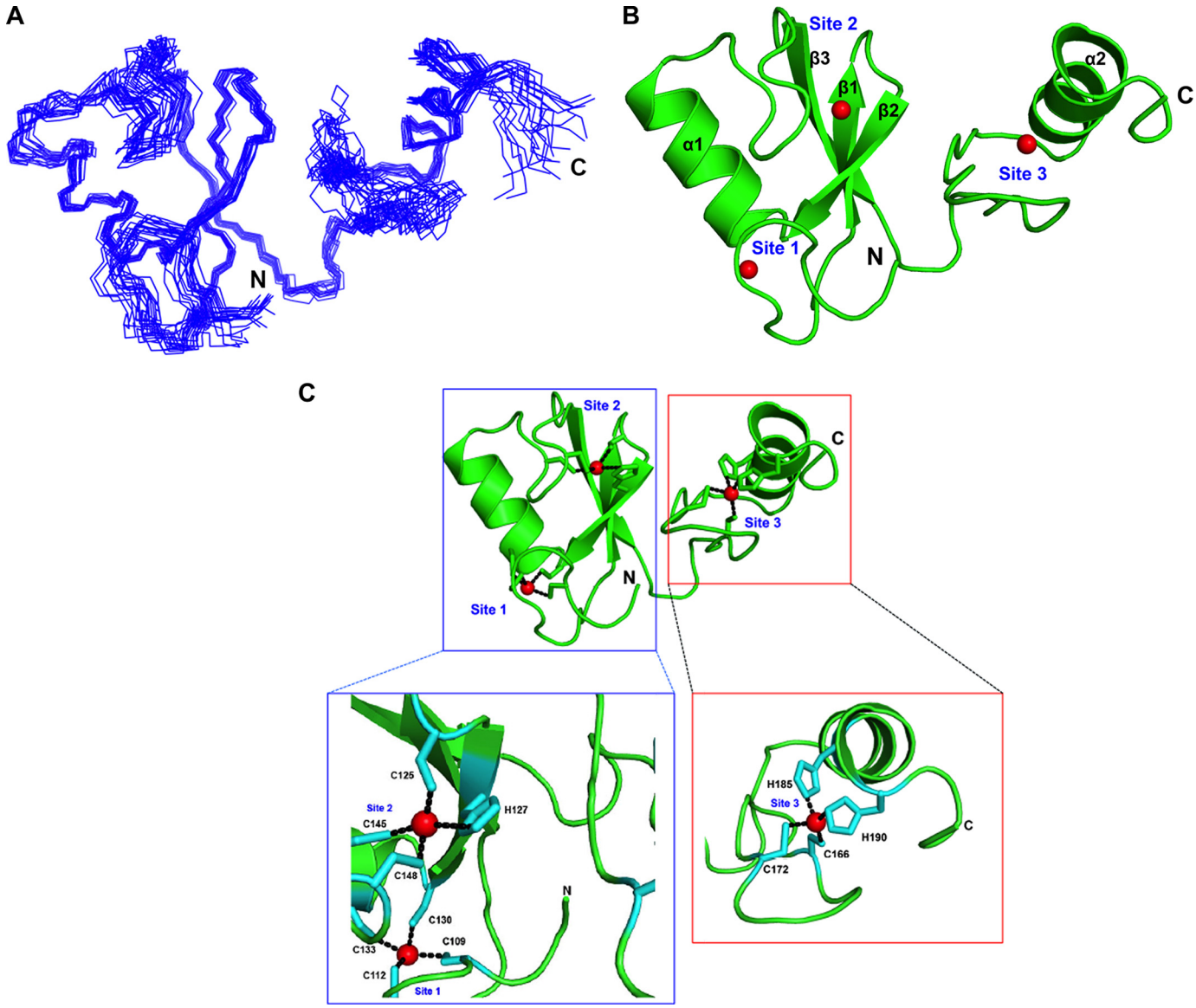

FIGURE 2. **NMR structure of HYB$^{\Delta C}$ (aa 106–194).** *A*, superposition of 20 energy-minimized conformers representing the NMR structure of HYB$^{\Delta C}$. *B*, ribbon diagram of the lowest-energy conformer representing the three-dimensional NMR structure of HYB$^{\Delta C}$. Each monomer contains three zinc-coordination sites: *Sites 1*, *2*, and *3*. The zinc ions are shown as *red spheres*. *C*, metal coordinations in the NMR structure of HYB$^{\Delta C}$. The coordination of zinc ions in the RING domain and the C-terminal domain of HYB$^{\Delta C}$ are shown.

(aa 106–194) sample prepared in the buffer containing 50 mM sodium phosphate, pH 6.5, and 5 mM DTT. ^{1}H, ^{13}C, and ^{15}N resonance assignments were achieved by measuring the three-dimensional HNCACB, three-dimensional CBCA(CO)NH (24), and three-dimensional CCH-TOCSY (25) spectra. Inter-proton distance restraints for structural calculation were obtained from three-dimensional ^{13}C-edited NOESY-HSQC, three-dimensional ^{15}N-edited NOESY-HSQC, and two-dimensional NOESY spectra using a 100-ms mixing time. A weakly aligned ^{15}N-labeled sample (0.8 mM) was prepared using the same buffer by the addition of 6 mg/ml of filamentous phage Pf1 (from ASLA Biotech Ltd, Latvia) for residue dipolar coupling (RDC) measurements. $^{1}D_{NH}$ RDCs were measured using the In-Phase and Anti-Phase method (26). The RDC values were obtained by subtracting the reference value in isotropic solution. NMR spectra (two- and three-dimensional) were processed using the NMRPipe program (27), and data analysis was performed with the help of the Sparky program (28).

Structure Determination—The solution structure for HYB$^{\Delta C}$ (aa 106–194) was calculated using the Xplor-NIH 2.24 software package (29). A total of 1087 NOE distance restraints, 21 hydrogen bonds, and 110 dihedral angle restraints were predicted by the TALOS program (30). Initial structures were calculated using torsion angle molecular dynamics protocol. Structure refinement was performed using a simulated annealing protocol, and 55 RDCs restraints were used in the cooling stage. The position of three zinc ions were determined by the distance restraints derived from the x-ray structure of HYB (PDB code 3VK6). The three zinc ions are bound to the HYB$^{\Delta C}$ through nine cysteines and three histidines exhibiting the topology Cys^{109}-X_2-Cys^{112}-Zn$_1$-Cys^{130}-X_2-Cys^{133}, Cys^{125}-X-His^{127}-Zn$_2$-Cys^{145}-X_2-Cys^{148}, and Cys^{166}-X_5-Cys^{172}-Zn$_3$-His^{185}-X_4-His^{190}, respec-

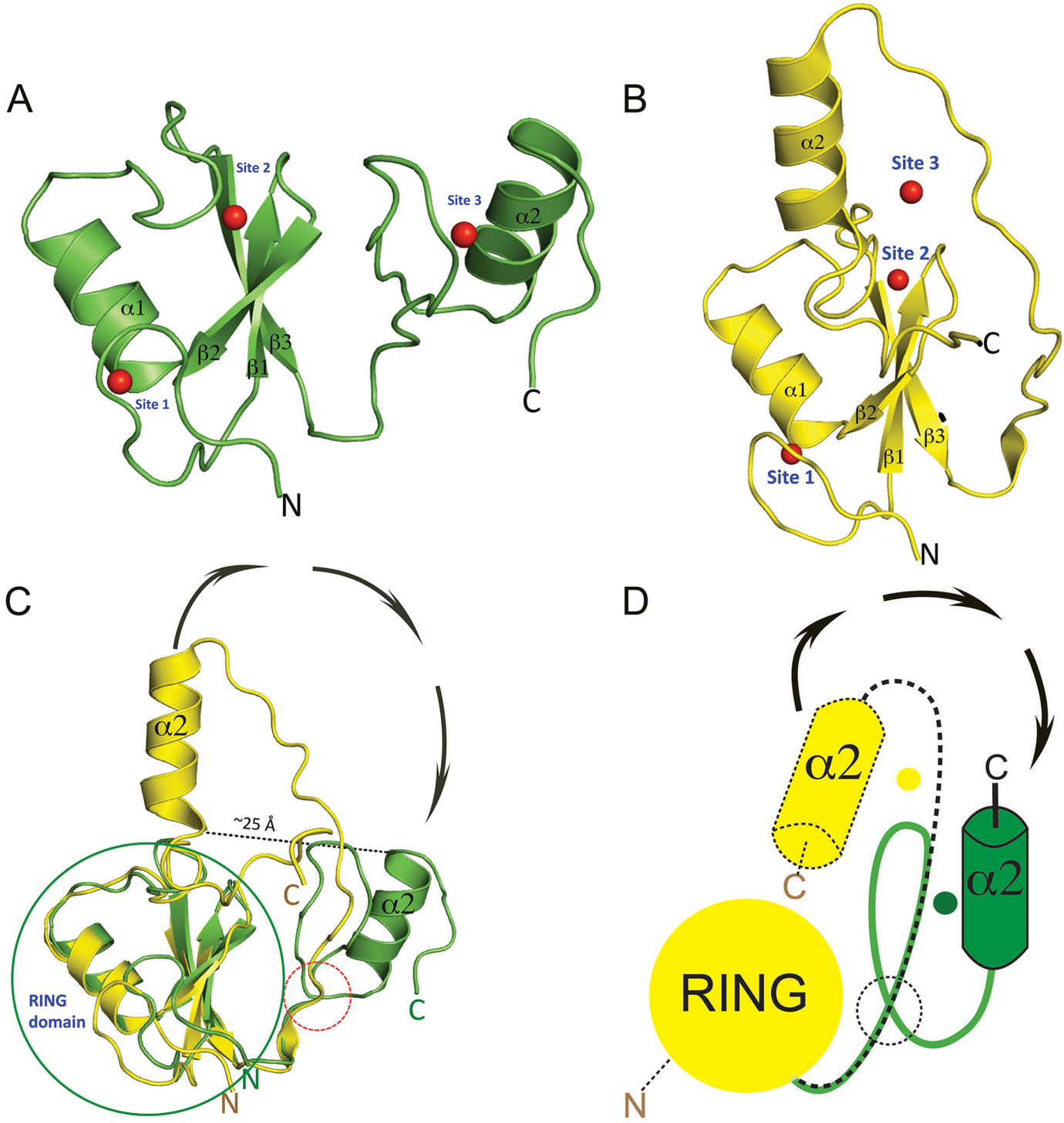

FIGURE 3. **Comparison of monomeric HYB$^{\Delta C}$ with monomeric Hakai of the dimeric HYB domain.** *A* and *B*, schematic representations of HYB$^{\Delta C}$ (aa 106–194; *green*) and the Hakai (aa 106–206; *yellow*) monomeric counterpart (PDB code 3vk6) of the HYB domain, respectively, in the same orientation. *C*, superposition of HYB$^{\Delta C}$ on Hakai reveals an overlap with a r.m.s. deviation of 0.9 Å for a stretch of residues from 106 to 166, which contains the RING domain and part of the C-terminal domain in both structures. Differences in the structure arise after residue Cys^{166} (highlighted by a *red dotted circle*, *lower right* of the figure). Beyond this, the folds of HYB$^{\Delta C}$ and the HYB monomeric counterpart are completely different, with the helix α2 flipping by 180° and separating by ~25 Å. The relative rotations that result in the conformational change are indicated by *arrows* orientated in a clockwise direction. *D*, schematic representation of the conformational changes in *C* of the structures of HYB$^{\Delta C}$ and Hakai (aa 106–206) of the HYB domain with the relative rotation resulting in the observed structural changes. The *yellow dot* represents the original position of the C-terminal zinc ion at Site 3 of the monomeric Hakai counterpart in the dimeric HYB domain, and the *green dot* represents the new position of the Site 3 zinc ion in HYB$^{\Delta C}$.

tively. These zinc ions were included in the structural calculations with an approximately tetrahedral geometry. The distance constraints include four fixed distances for each zinc ion, where the zinc-sulfur (cysteine S^{γ}) bond distance was set to 2.3 Å and zinc-nitrogen (histidine $N^{\epsilon 2}$) bond lengths was set to 2.0 Å, respectively. A final ensemble of the 20 lowest energy structures from 100 calculated structures was selected for the figure preparation using Chimera program.

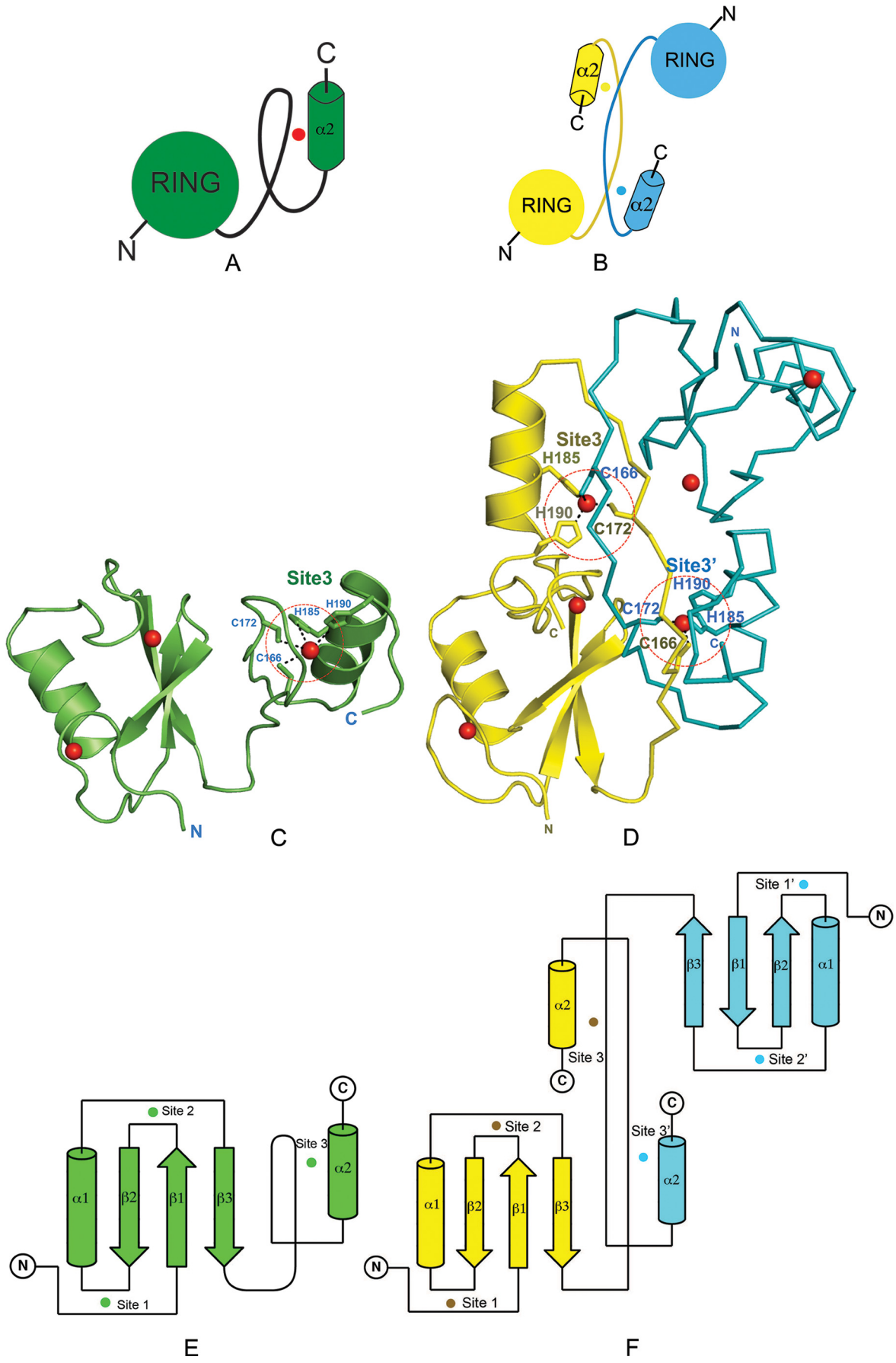
C
α2
RING
N
A
N
RING
α2
C
C
RING
α2
N
B
N
Site3
H185
C166
H190
C172
Site3'
H190
C172
H185
C166
C
C
N
D
Site3
H190
H185
C172
C166
C
N
C
Site 1'
N
β3
β1
β2
α1
α2
Site 3
Site 2'
C
Site 2
Site 3
C
α2
α1
β2
β1
β3
N
Site 1
E
Site 2
C
Site 3'
α2
α1
β2
β1
β3
N
Site 1
F

^{15}N Relaxation Measurements—The ^{15}N single-labeled free $HYB^{\Delta C}$ sample (0.8 mM) and complex sample (~1 mM peptide added) were used to measure the ^{15}N relaxation time, T_1 and T_2, respectively. The ^{15}N relaxation times, T_1 and $T_{1\rho}$, were measured at 25 °C using inversely detected two-dimensional NMR methods (31, 32) on a Bruker 800 Avance machine equipped with a TXI cryogenic probe. For the free $HYB^{\Delta C}$ sample, relaxation times, T_1, were determined by collecting eight points with delays of 10, 250 (×3), 400, 500, 650, 750, and 850 ms using a recycle delay of 3 s and 8 scans. Relaxation times, $T_{1\rho}$, were measured by collecting eight points with delays of 1, 30 (×2), 45, 60, 75, 90, and 110 ms using a spin-lock power of 1.6 kHz, a 2.0-s recycle delay, and 8 scans. For the complex sample, relaxation times, T_1, were determined by collecting eight points with delays of 10, 250 (×2), 400, 500, 650, 750, and 1000 ms using a recycle delay of 3 s and 16 scans. Relaxation times, $T_{1\rho}$, were measured by collecting eight points with delays of 1, 15, 30 (×2), 45, 60, 75, and 87 ms using a spin-lock power of 1.6 kHz, a 2.0-s recycle delay, and 16 scans. All data were recorded using 220 and 1280 complex points in t_1 and t_2 dimensions, respectively, and with spectral widths of 1946 Hz (^{15}N) and 11160 Hz (^{1}H). Relaxation times were fitted as single exponential decays to peak height data. The spin-spin relaxation time, T_2, was calculated from $T_{1\rho}$ and T_1 according to the following equation (32),

$$1/T_{1\rho} = 1/T_1 \sin^2\theta + 1/T_2 \cos^2\theta \qquad \text{(Eq. 2)}$$

where $\theta = \arctan(\Delta\omega/\omega_1)$, and $\Delta\omega$ and ω_1 are the resonance offset and spin-lock field strength, respectively. The experiment error was analyzed by repeating the T_1 measurement (250 ms) three times. The relative standard deviation for HSQC peak intensities was about 0.99%. The relaxation constants were also given with the fitting errors. The differences in relaxation parameters observed were significantly higher than the standard deviation; thus, it was outside the error range.

Isothermal Titration Calorimetry—The phosphorylated peptide of E-cadherin (residues 747–759) was titrated at a molar concentration of 575 μM against 75 μM $HYB^{\Delta C}$ in a VP-ITC microcalorimeter (Microcal, Northhampton, UK) at 293 K. The titrations were carried out using 30 10-μl injections of the peptide into the sample cell containing $HYB^{\Delta C}$ and the data were analyzed with a one-site binding model using the Origin software package version 7.0 supplied by Microcal. All measurements were repeated three times.

Analytical Ultracentrifugation (AUC)—The oligomeric states of the $HYB^{\Delta C}$ in the absence and presence of the Tyr(P) peptide were investigated by monitoring their sedimentation properties in AUC sedimentation velocity experiments. Samples (400 μl) in 50 mM sodium phosphate, pH 6.5, and 5 mM DTT with an absorbance of 1.0 at 280 nm were used. Sedimentation velocity profiles were collected by monitoring the absorbance at 280 nm. The samples were centrifuged at 40,000 × *g* at 25 °C in a Beckman ProteomeLab XL-I centrifuge fitted with a four-hole AN-60 Ti rotor and double-sector aluminum centerpieces and equipped with absorbance optics. The scans were analyzed using the Sedfit program (33).

Chemical Shift Perturbation Analysis—Chemical shift perturbations of backbone amides by the binding of phospho-E-cadherin-(747–759) peptide to $HYB^{\Delta C}$ (peptide to protein ratio is 1.2:1) were calculated. The chemical shift perturbations were defined as $\Delta\delta = [(\Delta\delta_{HN}{}^2 + \Delta\delta_N{}^2/25)/2]^{0.5}$ for amide NH, where $\Delta\delta_{HN}$ and $\Delta\delta_N$ are the chemical shift differences of amide ^{1}H, amide ^{15}N, between the samples in the presence of phospho-E-cadherin-(747–759) peptide and in the absence of phospho-E-cadherin-(747–759) peptide. The NH HSQC assignments for $HYB^{\Delta C}$ complex were confirmed by three-dimensional ^{15}N-edited NOESY-HSQC experiment.

RESULTS

$HYB^{\Delta C}$ Is a Monomer in Solution—We previously demonstrated that the HYB domain consists of an atypical zinc-coordinated, intertwined homodimer formed by an anti-parallel arrangement of two Hakai (aa 106–206) monomers (14). The dimerization mainly occurs through the C-terminal region of Hakai (aa 106–206), which harbors key Tyr(P)-interacting residues as well as the atypical zinc-coordinated motif formed by two histidine residues (His^{185} and His^{190}) and one cysteine residue (Cys^{172}) from one monomer and a second cysteine residue (Cys^{166}) from the adjacent monomer. In this study, we expressed and purified a C-terminal truncation mutant comprising residues 106–194, herein referred to as $HYB^{\Delta C}$, which retains all of the residues involved in the atypical zinc-coordinated motif and the Tyr(P) interaction. The gel-filtration elution profile showed that $HYB^{\Delta C}$ had an apparent molecular weight equivalent to a monomeric subunit (Fig. 1*A*). Furthermore, the monomeric nature of $HYB^{\Delta C}$ was verified using AUC analysis, which showed a peak corresponding to an apparent molecular mass of monomeric $HYB^{\Delta C}$ (~10,200 Da) (Fig. 1*B*). The dynamic light scattering experiments also revealed an apparent molecular weight of monomeric $HYB^{\Delta C}$.

Circular Dichroism Analysis—Circular dichroism (CD) analysis revealed significant differences in the secondary structure composition between the monomeric $HYB^{\Delta C}$ and the dimeric HYB domain (Fig. 1*C*). In the presence of the phosphorylated

FIGURE 4. **C_2H_2 ZnF in the C-terminal domain of $HYB^{\Delta C}$ is critical for its monomeric fold.** Analysis of the structural differences between $HYB^{\Delta C}$ and HYB (*A*) and the dimeric fold of HYB domain containing paired Hakai (aa 106–206) (PDB code 3vk6) monomers (*B*). The *red dot* in *A* represents the zinc ion in the C-terminal domain of $HYB^{\Delta C}$, whereas the *cyan* and *yellow dots* in *B* represent the C-terminal zinc ion shared between the respective monomers of the dimeric HYB-fold. *C,* the monomeric fold of $HYB^{\Delta C}$ (*green*) contains a C_2H_2 ZnF in the C-terminal domain (highlighted by *red dotted circle*). *D,* the HYB domain (PDB code 3vk6) contains a dimeric fold of paired Hakai (aa 106–206) monomers (*yellow* monomer in ribbon representation; *cyan* in schematic representation for clarity). In monomeric $HYB^{\Delta C}$, all four zinc-coordinating residues are situated in the same monomeric chain. Comparatively, the dimeric fold of the HYB domain is formed by the sharing of two zinc ions (*red spheres*) between the Hakai monomers, such that three of the four zinc-binding residues come from one monomer (His^{185}, His^{190}, and Cys^{172}) and the fourth from the adjacent monomer (Cys^{166}). The zinc-coordinating side chains are shown as *sticks*. The structural rearrangement arises because of a systematic reshuffling among the zinc-coordinating residues in the monomeric and dimeric conformers. Topology of $HYB^{\Delta C}$ (*E*) is compared with that of the HYB domain (PDB code 3vk6) (*F*). The zinc ions are shown as *spheres* (color coded according to the monomer colors) and the three zinc-coordination sites are indicated for each monomer (*Sites 1*, *2*, and *3*). In $HYB^{\Delta C}$, Site 3 is formed by four zinc-coordination residues, all situated from the same monomer. For the HYB domain, *Site 3* and *Site 3′* share residues from both monomers.

A

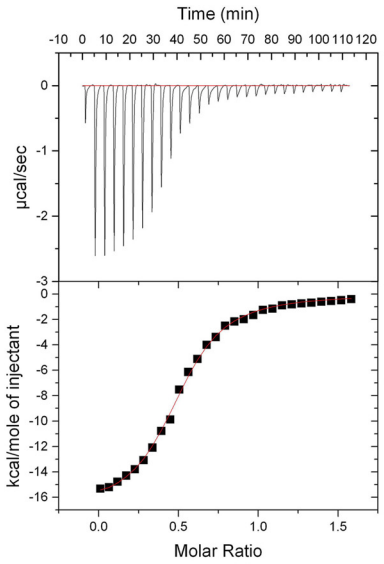

Peptide	Sequence	N	Ka (x10^6 M^{-1})	Kd (µM)	ΔH (kcal/mol)	TΔS (kcal/mol)	ΔG (kcal/mol)
E-cad$^{747-759}$	DTRNVYpYYDEEG	0.511± 0.004	0.2706± 0.014	3.7	-16.94± 0.165	-9.358	-7.582

B

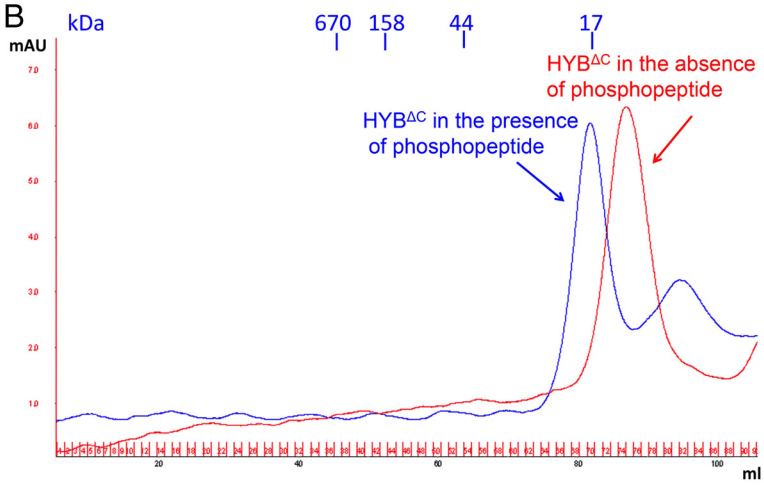

C

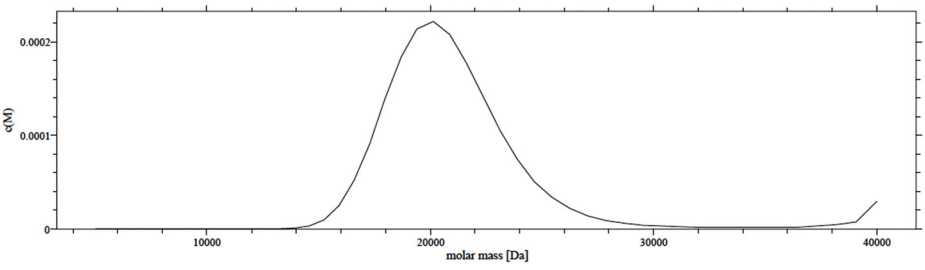

D

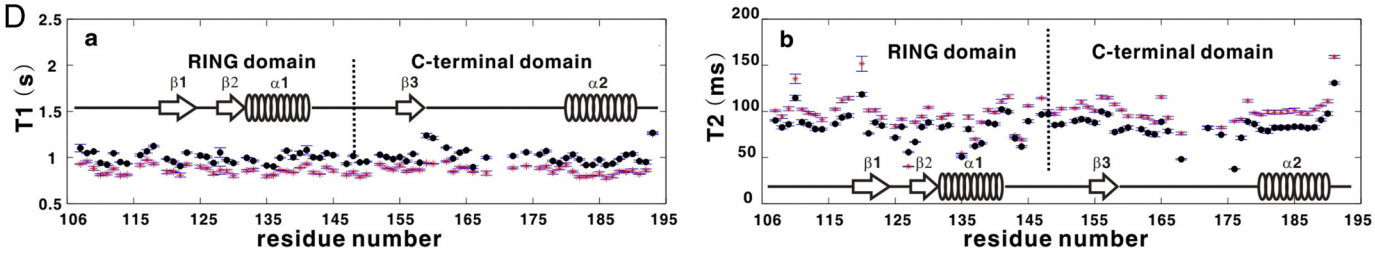

peptide of E-cadherin (corresponding to residues 747–759), the CD spectra demonstrated conformational changes to the $HYB^{\Delta C}$. These significant differences in the conformation of $HYB^{\Delta C}$ in the CD spectral analysis motivated us to determine the NMR structure of $HYB^{\Delta C}$ to understand the structural basis of this ligand-associated conformational change.

NMR Structure of $HYB^{\Delta C}$—To gain structural insights into the tertiary fold of $HYB^{\Delta C}$, we solved the solution NMR structure. The NMR structure of $HYB^{\Delta C}$ was refined to a final r.m.s. deviation of 0.63 ± 0.21 Å (backbone) (Table 1) for the 20 best structures (Fig. 2, *A* and *B*). The NMR structure of $HYB^{\Delta C}$ revealed a monomeric fold, comprising an N-terminal RING domain and a C-terminal zinc-coordinated domain bearing a C_2H_2-type zinc finger (ZnF) configuration (Fig. 2, *B* and *C*). As expected from knowledge of the HYB structure, the solution structure of $HYB^{\Delta C}$ contained three zinc-coordination sites. The RING domain (residues 106–148) was shown to adopt a typical RING architecture containing two β-strands (β1 and β2) and one α-helix (α1), which engage two zinc ions. The C-terminal domain (residues 148–194) lay in close association with the N-terminal RING domain by means of the third β-strand, β3, which formed an anti-parallel β-sheet arrangement with β1 and β2 of the RING domain. The C-terminal domain contained the third zinc-coordination site of $HYB^{\Delta C}$, formed by the residues Cys^{166}, Cys^{172}, His^{185}, and His^{190}, resembling a typical C_2H_2 ZnF motif (Fig. 2*C*); the two cysteines (Cys^{166} and Cys^{172}) formed a hairpin loop and the two histidines (His^{185} and His^{190}) were found juxtaposed to the α-helix (α2).

The overall structure of $HYB^{\Delta C}$ was compared with other proteins present in the Protein Data Bank using the DALI server (34). The DALI search showed several structural homologs containing a similar RING domain, but none bore any resemblance beyond amino acid residue 166 of the C-terminal domain of $HYB^{\Delta C}$, the C_2H_2 ZnF site. This suggested that combination of the N-terminal RING domain and the C-terminal domain containing the C_2H_2 ZnF adopts a novel fold in $HYB^{\Delta C}$. To determine whether any protein in the PDB database contained a fold resembling the C_2H_2 ZnF of $HYB^{\Delta C}$, a second DALI search was performed for the localized fold comprising amino acid residues 159–194 of $HYB^{\Delta C}$. The results showed only four proteins that contain a fold similar to the C_2H_2 ZnF of $HYB^{\Delta C}$: zinc finger protein 406 (PDB code 2elx), SPIF2 (PDB code 1sp2), RAS-related protein RAB-5A (PDB code 3mjh), and SWI5 (PDB code 1zfd), bearing a sequence similarity of 30, 27, 28, and 19%, and *Z*-scores of 2.4, 2.3, 2.1, and 2.1, respectively. These proteins are transcription factors, with the exception of RAB-5A, which is involved in Rab5 binding using the distinctive N-terminal C_2H_2 zinc finger (35).

Comparison of the Structure of $HYB^{\Delta C}$ with HYB Domain—To analyze the structural differences between monomeric $HYB^{\Delta C}$ and HYB domain, the monomeric $HYB^{\Delta C}$ was superimposed onto that of one of the monomeric counterparts of Hakai (aa 106–206). The structural segment corresponding to residues 106–166 of $HYB^{\Delta C}$ and one monomer of the HYB domain were found to be similar, with a r.m.s. deviation of 0.9 Å (Fig. 3). This implies that the RING domain (residues 106–148) and the fold of the linker sequence (residues 149–166) overlap in both $HYB^{\Delta C}$ and the monomer of the HYB domain. Structural differences arose, however, from residue 167 onward, which corresponds to the C-terminal zinc-coordination site and the terminal α-helix (α2). The C-terminal helix α2 of $HYB^{\Delta C}$ was flipped by 180° and is separated from the α2 of HYB monomeric counterpart by a distance of 25 Å (Fig. 3*C*). Fig. 4, *A–F*, show comparisons between the monomeric $HYB^{\Delta C}$ and the dimeric fold of the HYB domain. From these comparisons, it became apparent that the differences in the folding arose from changes in the C_2H_2 ZnF in $HYB^{\Delta C}$, with all of the zinc-coordination residues situated on the same monomeric chain of $HYB^{\Delta C}$; this is in contrast to the sharing of zinc ions between the two monomers in the atypical zinc-coordination motif of the HYB domain. Thus, the NMR structure provides the basis for the existence of $HYB^{\Delta C}$ as a monomer in solution and bearing a different fold, likely because its lacks the atypical zinc-binding motif, which is critical for the dimerization of the full-length HYB domain. The overall topology of $HYB^{\Delta C}$ and the HYB domain is compared in Fig. 4, *E* and *F*.

$HYB^{\Delta C}$ Binds Phospho-E-cadherin Ligand as a Dimer—We next questioned whether monomeric $HYB^{\Delta C}$ could still engage with a phosphorylated substrate ligand. Hence, we conducted isothermal titration calorimetry (ITC) experiments to investigate the binding property of $HYB^{\Delta C}$ with the peptide ligand corresponding to our previously established Tyr(P) motif of E-cadherin, comprising residues 747–759 (14). The ITC experiment revealed that $HYB^{\Delta C}$ binds with the Tyr(P) ligand of E-cadherin with a binding stoichiometry of 2:1 ($HYB^{\Delta C}$:Tyr(P) ligand) and an affinity value of K_d = 3.7 μM (Fig. 5*A*). This indicates that the phospho-E-cadherin-(747–759) ligand interacts with a dimeric form of $HYB^{\Delta C}$.

To further understand the dimeric nature of this interaction, $HYB^{\Delta C}$ was separated on a calibrated gel-filtration column in the presence and absence of the ligand. A comparison of these two elution profiles showed that $HYB^{\Delta C}$ elutes as a dimer in the presence of the ligand and as a monomer in its *apo* form (Fig. 5*B*). To further verify this presumed ligand-induced dimerization of $HYB^{\Delta C}$, sedimentation velocity AUC experiments were conducted with the samples containing $HYB^{\Delta C}$ in the presence

FIGURE 5. **ITC, gel filtration profiles, AUC, and NMR relaxation studies of $HYB^{\Delta C}$ with phospho-E-cadherin-(747–759).** *A,* the tyrosine-phosphorylated E-cadherin-(747–759) was titrated against $HYB^{\Delta C}$ using ITC. The *top panel* shows the heat release profile after baseline correction and the *lower panel* indicates the binding isotherm for the interaction. The dissociation constant (K_d) and binding stoichiometry (*N*) are shown in the table. *B,* comparison of gel filtration profiles of $HYB^{\Delta C}$ in the presence (*blue*) and absence (*red*) of phospho-E-cadherin-(747–759) using a Superdex 75 gel filtration column. The elution profile suggests that $HYB^{\Delta C}$ exists as a dimer in the presence of ligand but as a monomer in the absence of the ligand. *C,* AUC analysis of $HYB^{\Delta C}$ in the presence of phospho-E-cadherin-(747–759) ligand. The ligand-induced dimerization of $HYB^{\Delta C}$ was studied using sedimentation velocity analysis. The results show that the protein exists as a dimer in the presence of the ligand with an apparent molecular mass of 20,000 Da. *D,* ^{15}N relaxation T_1 (*a*) and T_2 (*b*) values as well as the error values for each residues in free $HYB^{\Delta C}$ sample (labeled as a *red star*) and phospho-E-cadherin$^{747–759}$ bound complex (labeled as ●). The results show the T_1 and T_2 values change in the presence and absence of the substrate peptide. The secondary structures and domain boundary of $HYB^{\Delta C}$ also are illustrated in the *middle* of the figure. The missing residues and weak intensity residues (except Val^{128}) are located in the region between β3 and α2.

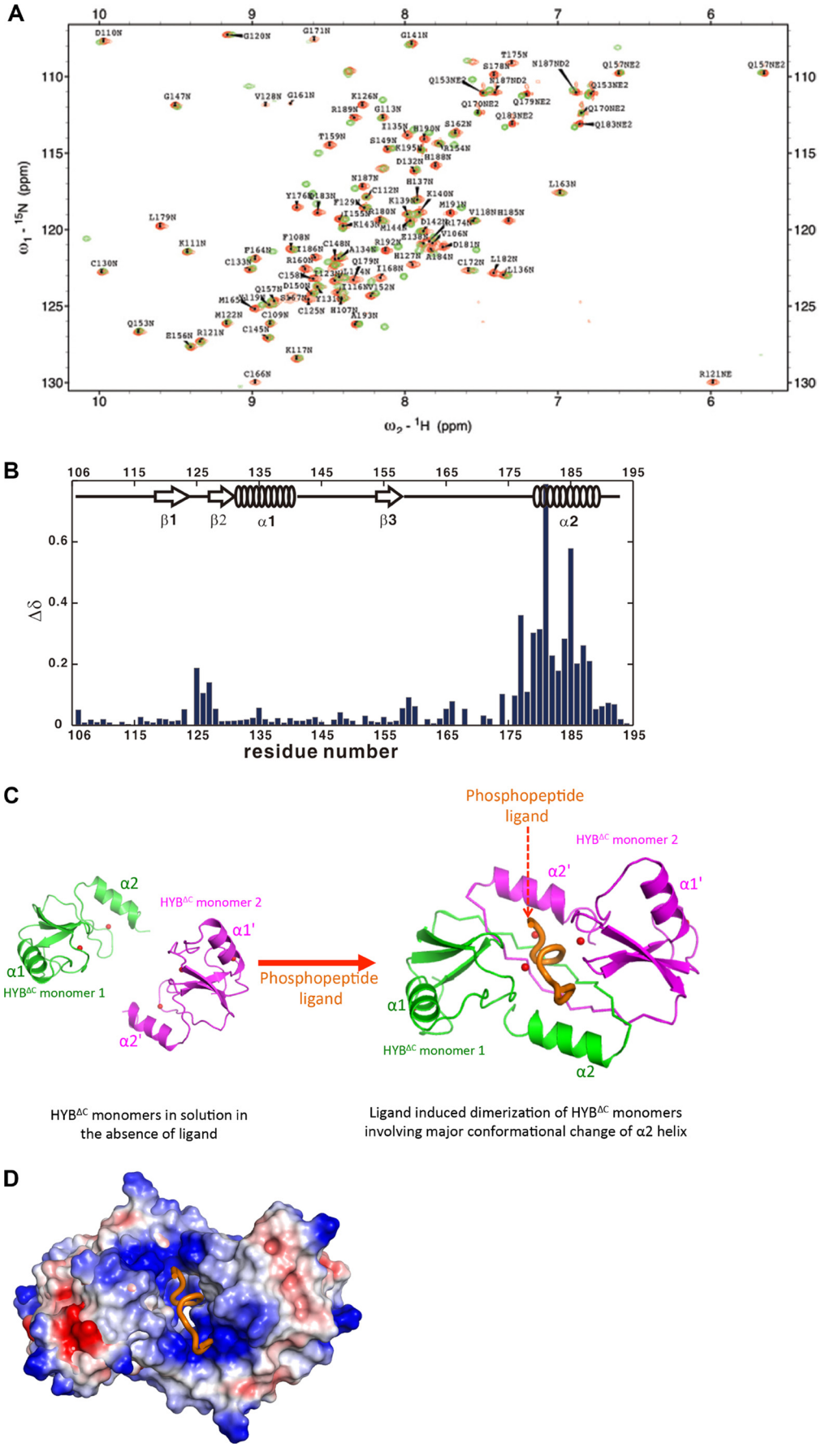
A
ω_1 - ^{15}N (ppm)
ω_2 - ^{1}H (ppm)
B
β1
β2
α1
β3
α2
Δδ
residue number
C
HYB$^{\Delta C}$ monomer 1
HYB$^{\Delta C}$ monomer 2
α1
α2
α1'
α2'
Phosphopeptide ligand
HYB$^{\Delta C}$ monomers in solution in the absence of ligand
Ligand induced dimerization of HYB$^{\Delta C}$ monomers involving major conformational change of α2 helix
D

of the phospho-E-cadherin-(747–759) peptide. The analysis of the AUC data using Sedfit (33) showed that the apparent molecular mass of $HYB^{\Delta C}$ in the presence of ligand is 20,000 Da (Fig. 5*C*), which is equivalent to twice the monomeric molecular weight of $HYB^{\Delta C}$. Interestingly, the ^{15}N relaxation data clearly showed a change in the T_1 and T_2 values in the presence and absence of the substrate peptide (Fig. 5*D*). The average T_1 and T_2 values for the free $HYB^{\Delta C}$ were 0.88 s and 120 ms, respectively. However, upon binding to the peptide, the average T_1 and T_2 values for the complex were 1.02 s and 100 ms, respectively. These results indicate that a high molecular weight complex is formed upon binding. Dynamic light scattering results further confirmed these findings, with an apparent molecular weight corresponding to a dimer in the presence of the substrate peptide. The combined results suggest that $HYB^{\Delta C}$ switches from a monomeric conformation to a dimeric form in the presence of a Tyr(P)-containing ligand.

Proposed Model of Tyr(P) Recognition by $HYB^{\Delta C}$—To understand the mode of Tyr(P) recognition by $HYB^{\Delta C}$, we undertook chemical shift perturbation analyses of $HYB^{\Delta C}$ in the presence of phospho-E-cadherin-(747–759). The results showed a significant shift for α2 helix in the presence of phospho-E-cadherin-(747–759) (Fig. 6, *A* and *B*). This chemical shift perturbation upon ligand binding with $HYB^{\Delta C}$ bears marked similarity to the one observed in our previous study wherein the ^{15}N dimeric HYB domain was titrated with the phospho-E-cadherin-(747–759) peptide (14). Given that the presence of a Tyr(P) ligand changes the oligomerization, we analyzed the proposed dimeric configuration formed by the $HYB^{\Delta C}$ monomers in the presence of Tyr(P) ligand. We compared the $HYB^{\Delta C}$ monomer structure with the corresponding monomer of the untruncated HYB domain and observed a major conformational change in the α2 helix of the $HYB^{\Delta C}$ (Figs. 3 and 4). Our observations from the solution experiments, structural analysis, chemical shift perturbation data, and previous mutational data (14) suggest that the Tyr(P) ligand induces the dimerization to create a binding pocket in $HYB^{\Delta C}$ for substrate recognition (Fig. 6*C*). The electrostatic surface potential representation of $HYB^{\Delta C}$ in the phospho-E-cadherin-(747–759) peptide complex model suggests that the Tyr(P) along with the surrounding acidic residues on the phospho-E-cadherin-(747–759) peptide potentially interact with the positively charged $HYB^{\Delta C}$ binding pocket (Fig. 6*D*).

DISCUSSION

Phosphotyrosine-binding domains are critical, modular components that bind to phosphorylated tyrosine residues in acceptor proteins to create multiprotein complexes and regulate several intracellular signaling pathways (1, 8, 36). Dysregulation of these pathways is often associated with oncogenic transformation (37), rendering Tyr(P)-binding domains as attractive targets for directed therapies (38–40). So far, all of the major Tyr(P)-binding domains, including SH2 and phosphotyrosine-binding domains, tend to be monomeric (7, 41), barring the few exceptions where they function as homodimers. These exceptions include the SH2 domains of Grb10, Grb14, Grb7, APS, and SH2-B (7, 41–43). In addition, in STAT proteins, tyrosine phosphorylation mediated dimerization has been reported to occur via SH2 domains (44–46). The recently identified Tyr(P)-binding fold in Hakai, HYB, bears a novel dimeric fold consisting of two atypical ZnFs shared between the paired Hakai (aa 106–206) monomers that exist in an intertwined configuration across the flexible C-terminal region (14). Previously we showed that the atypical, intermolecular zinc coordination is necessary for the dimerization of Hakai and hence its ability to interact with the substrate (14). Mutations of these residues involved in intermolecular zinc coordination results in dimer to monomer transition; and also abrogate the ability of full-length Hakai to bind its targets like E-cadherin and Cortactin, as revealed in the mammalian cell based studies (14). In this study, we showed that deletion of the flexible C-terminal region of HYB also results a monomeric fold in solution. A similar observation was recently reported in the C-terminal domain of SARS-CoV main protease (M^{pro}-C), where the truncation of the disordered C-terminal helix results in its transition from a dimer to a monomer (47). In yet another study, a dimer/tetramer equilibrium observed in *Escherichia coli* DNA mismatch repair protein MutS is converted into a monomer/dimer equilibrium upon deletion of the C-terminal 53 amino acids (48).

To understand the structural basis for this monomeric conformation of $HYB^{\Delta C}$, we determined its solution NMR structure. The NMR structure revealed that the characteristic atypical ZnF, which plays a key role in the dimeric fold of the HYB domain, is replaced by a C_2H_2-type ZnF in $HYB^{\Delta C}$, formed by two cysteines and two histidines, all situated on the same monomer. This represents a unique monomeric to dimeric switching mechanism.

One of the best studied physiological functions of the HYB domain is its interaction with and regulation of tyrosine-phosphorylated E-cadherin at cell-cell junctions (14, 15, 49, 50). As such, we selected a tyrosine-phosphorylated E-cadherin-(747–759) peptide as a model substrate to further assess this mono-

FIGURE 6. **Proposed model of Tyr(P) recognition by $HYB^{\Delta C}$.** *A*, an overlay of the HN-HSQC spectra of $HYB^{\Delta C}$ in the absence (*green*) or presence (*red*) of phospho-E-cadherin-(747–759) peptide. *B,* chemical shift perturbations of backbone amides by the binding of phospho-E-cadherin-(747–759) peptide to $HYB^{\Delta C}$. The chemical shift perturbations were defined as $\Delta\delta = [(\Delta\delta_{HN}^2 + \Delta\delta_N^2/25)/2]^{0.5}$ for amide NH, where $\Delta\delta_{HN}$ and $\Delta\delta_N$ are the chemical shift differences of amide ^1H, amide ^{15}N, between the samples in the presence and absence of phospho-E-cadherin-(747–759) peptide. The NH HSQC assignments for $HYB^{\Delta C}$ complex were confirmed by three-dimensional ^{15}N-edited NOESY-HSQC experiment. The empty regions represent no information available for residues in those regions because the NH HSQC peaks of those residues were invisible or unassigned. The secondary structures of $HYB^{\Delta C}$ also are illustrated in the *middle* of the figure. *C,* a proposed model of Tyr(P) recognition by the ligand-induced dimeric configuration of the $HYB^{\Delta C}$ monomers. The respective monomers are shown in *green* and *magenta*, with the peptide ligand in *orange*. The zinc ions are shown as *red spheres*. The $HYB^{\Delta C}$·Tyr(P) peptide complex model was generated based on the chemical shift data as well as our previous mutational and binding studies (14), which showed the interaction of His^{127}, Tyr^{176}, His^{185}, and Arg^{189} of HYB with the E-cadherin. Although the interacting side chains from the Tyr(P) peptide are not yet clearly established, our previous mutational studies showed that Asp^{750}, Val^{752}, $Tyr(P)^{754}$, Asp^{756}, and Glu^{757} are the interacting sites from the phospho-E-cadherin-(747–759) peptide (14). *D*, an electrostatic surface potential representation of the model presented in *C* suggests that the Tyr(P) along with its surrounding acidic residues of the phospho-E-cadherin-(747–759) interacts with the positively charged $HYB^{\Delta C}$ binding pocket. The Tyr(P) peptide ligand is shown in *orange*.

meric conformation of $HYB^{\Delta C}$ and to determine whether it is still functional. The ITC interaction studies showed that the ligand binds with the protein only in its dimeric form. This result is consistent with our previous studies that a dimeric HYB fold is necessary to create the Tyr(P) binding pocket; this was also validated with full-length Hakai in cell-based experiments (14). A series of solution studies further validated this switch to a dimeric conformation of $HYB^{\Delta C}$ in the presence of the Tyr(P) E-cadherin-(747–759) ligand. Furthermore, all of these experiments were carried out at different concentrations of $HYB^{\Delta C}$ and suggest that the ligand-induced dimerization of $HYB^{\Delta C}$ is independent of protein concentration. Previous studies have demonstrated ligand-mediated dimerization as a novel mechanism for protein-carbohydrate recognition (51, 52). The present study extends upon this paradigm to Tyr(P) signaling and regulation in Hakai.

Protein dimerization is an important regulatory mechanism in signal transduction (53–55). Numerous RING finger ubiquitin ligase family members require dimerization for their function; for example, cIAP, XIAP, RNF4, SIAH, and TRAF2 act as homodimers (56–60), whereas heterodimers form between MDM2 and MDMX, BRCA1 and BARD1, and RING1b and BMI1, respectively (61). Previous studies have shown that dimerization is often necessary for the interaction of the E2 ubiquitin conjugate with the RING domain (56). However, the dimerization of Hakai monomers reported in this study likely represents a unique mechanism, as the incoming substrate, rather than association with the RING domain, mediates the dimerization. This might represent a critical mechanism to facilitate the conformational switch Hakai requires for substrate binding and thus for the ubiquitination of the substrates such as E-cadherin.

In conclusion, we have identified a novel monomeric fold of $HYB^{\Delta C}$, which impairs its Tyr(P) binding property. However, in the presence of the Tyr(P) ligand, the monomeric $HYB^{\Delta C}$ becomes a dimer to create the Tyr(P) binding pocket to engage the substrate. The findings from this study suggest that the dimeric architecture of the HYB domain is necessary to engage the Tyr(P) ligand, which is in sharp contrast to all the other known Tyr(P)-binding domains that predominantly function as monomers. Selectively targeting the dimeric interface of therapeutically important enzymes has emerged as an attractive method of allosteric inhibition (62–65). The importance of the dimeric architecture of HYB in Tyr(P) substrate binding demonstrated by the present study makes it an ideal target for the design of selective allosteric inhibitors that abrogate HYB dimerization and potentially act as novel therapeutic interventions against cancer.

REFERENCES

1. Yaffe, M. B. (2002) Phosphotyrosine-binding domains in signal transduction. *Nat. Rev. Mol. Cell Biol.* **3,** 177–186
2. Deribe, Y. L., Pawson, T., and Dikic, I. (2010) Post-translational modifications in signal integration. *Nat. Struct. Mol. Biol.* **17,** 666–672
3. Hunter, T. (2009) Tyrosine phosphorylation: thirty years and counting. *Curr. Opin. Cell Biol.* **21,** 140–146
4. DeClue, J. E., Sadowski, I., Martin, G. S., and Pawson, T. (1987) A conserved domain regulates interactions of the v-fps protein-tyrosine kinase with the host cell. *Proc. Natl. Acad. Sci. U.S.A.* **84,** 9064–9068
5. Sadowski, I., Stone, J. C., and Pawson, T. (1986) A noncatalytic domain conserved among cytoplasmic protein-tyrosine kinases modifies the kinase function and transforming activity of Fujinami sarcoma virus P130gag-fps. *Mol. Cell. Biol.* **6,** 4396–4408
6. Forman-Kay, J. D., and Pawson, T. (1999) Diversity in protein recognition by PTB domains. *Curr. Opin. Struct. Biol.* **9,** 690–695
7. Liu, B. A., Jablonowski, K., Raina, M., Arcé, M., Pawson, T., and Nash, P. D. (2006) The human and mouse complement of SH2 domain proteins-establishing the boundaries of phosphotyrosine signaling. *Mol. Cell* **22,** 851–868
8. Pawson, T., and Nash, P. (2003) Assembly of cell regulatory systems through protein interaction domains. *Science* **300,** 445–452
9. Songyang, Z., Shoelson, S. E., Chaudhuri, M., Gish, G., Pawson, T., Haser, W. G., King, F., Roberts, T., Ratnofsky, S., and Lechleider, R. J. (1993) SH2 domains recognize specific phosphopeptide sequences. *Cell* **72,** 767–778
10. Filippakopoulos, P., Müller, S., and Knapp, S. (2009) SH2 domains: modulators of nonreceptor tyrosine kinase activity. *Curr. Opin. Struct. Biol.* **19,** 643–649
11. Kavanaugh, W. M., and Williams, L. T. (1994) An alternative to SH2 domains for binding tyrosine-phosphorylated proteins. *Science* **266,** 1862–1865
12. Benes, C. H., Wu, N., Elia, A. E., Dharia, T., Cantley, L. C., and Soltoff, S. P. (2005) The C2 domain of PKCδ is a phosphotyrosine binding domain. *Cell* **121,** 271–280
13. Christofk, H. R., Vander Heiden, M. G., Wu, N., Asara, J. M., and Cantley, L. C. (2008) Pyruvate kinase M2 is a phosphotyrosine-binding protein. *Nature* **452,** 181–186
14. Mukherjee, M., Chow, S. Y., Yusoff, P., Seetharaman, J., Ng, C., Sinniah, S., Koh, X. W., Asgar, N. F., Li, D., Yim, D., Jackson, R. A., Yew, J., Qian, J., Iyu, A., Lim, Y. P., Zhou, X., Sze, S. K., Guy, G. R., and Sivaraman, J. (2012) Structure of a novel phosphotyrosine-binding domain in Hakai that targets E-cadherin. *EMBO J.* **31,** 1308–1319
15. Fujita, Y., Krause, G., Scheffner, M., Zechner, D., Leddy, H. E., Behrens, J., Sommer, T., and Birchmeier, W. (2002) Hakai, a c-Cbl-like protein, ubiquitinates and induces endocytosis of the E-cadherin complex. *Nat. Cell Biol.* **4,** 222–231
16. Pece, S., and Gutkind, J. S. (2002) E-cadherin and Hakai: signalling, remodeling or destruction? *Nat. Cell Biol.* **4,** E72–E74
17. Figueroa, A., Kotani, H., Toda, Y., Mazan-Mamczarz, K., Mueller, E. C., Otto, A., Disch, L., Norman, M., Ramdasi, R. M., Keshtgar, M., Gorospe, M., and Fujita, Y. (2009) Novel roles of hakai in cell proliferation and oncogenesis. *Mol. Biol. Cell* **20,** 3533–3542
18. Abella, V., Valladares, M., Rodriguez, T., Haz, M., Blanco, M., Tarrío, N., Iglesias, P., Aparicio, L. A., and Figueroa, A. (2012) miR-203 regulates cell proliferation through its influence on Hakai expression. *PloS One* **7,** e52568
19. Wu, H., Reynolds, A. B., Kanner, S. B., Vines, R. R., and Parsons, J. T. (1991) Identification and characterization of a novel cytoskeleton-associated $pp60^{src}$ substrate. *Mol. Cell. Biol.* **11,** 5113–5124
20. Mashima, R., Hishida, Y., Tezuka, T., and Yamanashi, Y. (2009) The roles of Dok family adapters in immunoreceptor signaling. *Immunol. Rev.* **232,** 273–285
21. Noh, S. J., Baek, H. A., Park, H. S., Jang, K. Y., Moon, W. S., Kang, M. J., Lee, D. G., Kim, M. H., Lee, J. H., and Chung, M. J. (2013) Expression of SIRT1 and cortactin is associated with progression of non-small cell lung cancer. *Pathol. Res. Pract.* **209,** 365–370
22. Siouda, M., Yue, J., Shukla, R., Guillermier, S., Herceg, Z., Creveaux, M., Accardi, R., Tommasino, M., and Sylla, B. S. (2012) Transcriptional regulation of the human tumor suppressor DOK1 by E2F1. *Mol. Cell. Biol.* **32,** 4877–4890
23. Whitmore, L., and Wallace, B. A. (2008) Protein secondary structure analyses from circular dichroism spectroscopy: methods and reference databases. *Biopolymers* **89,** 392–400
24. Bax, A., and Grzesiek, S. (1993) Methodological advances in protein NMR. *Acc. Chem. Res.* **26,** 131–138
25. Fesik, S. W., Eaton, H. L., Olejniczak, E. T., Zuiderweg, E. R. P., McIntosh, L. P., and Dahlquist, F. W. (1990) 2D and 3D NMR spectroscopy employing carbon-13/carbon-13 magnetization transfer by isotropic mixing: spin

system identification in large proteins. *J. Am. Chem. Soc.* **112,** 886–888
26. Ottiger, M., Delaglio, F., and Bax, A. (1998) Measurement of J and dipolar couplings from simplified two-dimensional NMR spectra. *J. Magn. Reson.* **131,** 373–378
27. Delaglio, F., Grzesiek, S., Vuister, G. W., Zhu, G., Pfeifer, J., and Bax, A. (1995) NMRPipe: a multidimensional spectral processing system based on UNIX pipes. *J. Biomol. NMR* **6,** 277–293
28. Goddard, T. D., and Kneller, D. G. (2004) *SPARKY 3.* University of California, San Francisco, CA
29. Schwieters, C. D., Kuszewski, J. J., Tjandra, N., and Clore, G. M. (2003) The Xplor-NIH NMR molecular structure determination package. *J. Magn. Reson.* **160,** 65–73
30. Cornilescu, G., Delaglio, F., and Bax, A. (1999) Protein backbone angle restraints from searching a database for chemical shift and sequence homology. *J. Biomol. NMR* **13,** 289–302
31. Farrow, N. A., Muhandiram, R., Singer, A. U., Pascal, S. M., Kay, C. M., Gish, G., Shoelson, S. E., Pawson, T., Forman-Kay, J. D., and Kay, L. E. (1994) Backbone dynamics of a free and phosphopeptide-complexed Src homology 2 domain studied by ^{15}N NMR relaxation. *Biochemistry* **33,** 5984–6003
32. Akke, M., and Palmer, A. G. (1996) Monitoring macromolecular motions on microsecond to millisecond time scales by R1ρ-R1 constant relaxation time NMR spectroscopy. *J. Am. Chem. Soc.* **118,** 911–912
33. Brown, P. H., and Schuck, P. (2006) Macromolecular size-and-shape distributions by sedimentation velocity analytical ultracentrifugation. *Biophys. J.* **90,** 4651–4661
34. Holm, L., Kääriäinen, S., Rosenström, P., and Schenkel, A. (2008) Searching protein structure databases with DaliLite v.3. *Bioinformatics* **24,** 2780–2781
35. Mishra, A., Eathiraj, S., Corvera, S., and Lambright, D. G. (2010) Structural basis for Rab GTPase recognition and endosome tethering by the C2H2 zinc finger of early endosomal autoantigen 1 (EEA1). *Proc. Natl. Acad. Sci. U.S.A.* **107,** 10866–10871
36. Evans, J. V., Ammer, A. G., Jett, J. E., Bolcato, C. A., Breaux, J. C., Martin, K. H., Culp, M. V., Gannett, P. M., and Weed, S. A. (2012) Src binds cortactin through an SH2 domain cystine-mediated linkage. *J. Cell Sci.* **125,** 6185–6197
37. Pawson, T. (2002) Regulation and targets of receptor tyrosine kinases. *Eur. J. Cancer* **38,** S3–S10
38. Burke, T. R., Jr., Yao, Z. J., Liu, D. G., Voigt, J., and Gao, Y. (2001) Phosphoryltyrosyl mimetics in the design of peptide-based signal transduction inhibitors. *Biopolymers* **60,** 32–44
39. Machida, K., and Mayer, B. J. (2005) The SH2 domain: versatile signaling module and pharmaceutical target. *Biochim. Biophys. Acta* **1747,** 1–25
40. Sawyer, T. K., Bohacek, R. S., Dalgarno, D. C., Eyermann, C. J., Kawahata, N., Metcalf, C. A., 3rd, Shakespeare, W. C., Sundaramoorthi, R., Wang, Y., and Yang, M. G. (2002) SRC homology-2 inhibitors: peptidomimetic and nonpeptide. *Mini Rev. Med. Chem.* **2,** 475–488
41. Stein, E. G., Ghirlando, R., and Hubbard, S. R. (2003) Structural basis for dimerization of the Grb10 Src homology 2 domain. Implications for ligand specificity. *J. Biol. Chem.* **278,** 13257–13264
42. Depetris, R. S., Hu, J., Gimpelevich, I., Holt, L. J., Daly, R. J., and Hubbard, S. R. (2005) Structural basis for inhibition of the insulin receptor by the adaptor protein Grb14. *Mol. Cell* **20,** 325–333
43. Hu, J., and Hubbard, S. R. (2005) Structural characterization of a novel Cbl phosphotyrosine recognition motif in the APS family of adapter proteins. *J. Biol. Chem.* **280,** 18943–18949
44. Darnell, J. E., Jr. (1997) STATs and gene regulation. *Science* **277,** 1630–1635
45. Soler-Lopez, M., Petosa, C., Fukuzawa, M., Ravelli, R., Williams, J. G., and Müller, C. W. (2004) Structure of an activated *Dictyostelium* STAT in its DNA-unbound form. *Molecular cell* **13,** 791–804
46. Wenta, N., Strauss, H., Meyer, S., and Vinkemeier, U. (2008) Tyrosine phosphorylation regulates the partitioning of STAT1 between different dimer conformations. *Proc. Natl. Acad. Sci. U.S.A.* **105,** 9238–9243
47. Kang, X., Zhong, N., Zou, P., Zhang, S., Jin, C., and Xia, B. (2012) Foldon unfolding mediates the interconversion between M(pro)-C monomer and 3D domain-swapped dimer. *Proc. Natl. Acad. Sci. U.S.A.* **109,** 14900–14905
48. Manelyte, L., Urbanke, C., Giron-Monzon, L., and Friedhoff, P. (2006) Structural and functional analysis of the MutS C-terminal tetramerization domain. *Nucleic Acids Res.* **34,** 5270–5279
49. Ishiyama, N., and Ikura, M. (2012) The three-dimensional structure of the cadherin-catenin complex. *Subcell. Biochem.* **60,** 39–62
50. Ishiyama, N., Lee, S. H., Liu, S., Li, G. Y., Smith, M. J., Reichardt, L. F., and Ikura, M. (2010) Dynamic and static interactions between p120 catenin and E-cadherin regulate the stability of cell-cell adhesion. *Cell* **141,** 117–128
51. Flint, J., Nurizzo, D., Harding, S. E., Longman, E., Davies, G. J., Gilbert, H. J., and Bolam, D. N. (2004) Ligand-mediated dimerization of a carbohydrate-binding molecule reveals a novel mechanism for protein-carbohydrate recognition. *J. Mol. Biol.* **337,** 417–426
52. Sánchez-Vallet, A., Saleem-Batcha, R., Kombrink, A., Hansen, G., Valkenburg, D. J., Thomma, B. P., and Mesters, J. R. (2013) Fungal effector Ecp6 outcompetes host immune receptor for chitin binding through intrachain LysM dimerization. *eLife* **2,** e00790
53. Austin, D. J., Crabtree, G. R., and Schreiber, S. L. (1994) Proximity versus allostery: the role of regulated protein dimerization in biology. *Chem. Biol.* **1,** 131–136
54. Klemm, J. D., Schreiber, S. L., and Crabtree, G. R. (1998) Dimerization as a regulatory mechanism in signal transduction. *Annu. Rev. Immunol.* **16,** 569–592
55. Marianayagam, N. J., Sunde, M., and Matthews, J. M. (2004) The power of two: protein dimerization in biology. *Trends Biochem. Sci.* **29,** 618–625
56. Nakatani, Y., Kleffmann, T., Linke, K., Condon, S. M., Hinds, M. G., and Day, C. L. (2013) Regulation of ubiquitin transfer by XIAP, a dimeric RING E3 ligase. *Biochem. J.* **450,** 629–638
57. Liew, C. W., Sun, H., Hunter, T., and Day, C. L. (2010) RING domain dimerization is essential for RNF4 function. *Biochem. J.* **431,** 23–29
58. Mace, P. D., Linke, K., Feltham, R., Schumacher, F. R., Smith, C. A., Vaux, D. L., Silke, J., and Day, C. L. (2008) Structures of the cIAP2 RING domain reveal conformational changes associated with ubiquitin-conjugating enzyme (E2) recruitment. *J. Biol. Chem.* **283,** 31633–31640
59. Park, Y. C., Burkitt, V., Villa, A. R., Tong, L., and Wu, H. (1999) Structural basis for self-association and receptor recognition of human TRAF2. *Nature* **398,** 533–538
60. Polekhina, G., House, C. M., Traficante, N., Mackay, J. P., Relaix, F., Sassoon, D. A., Parker, M. W., and Bowtell, D. D. (2002) Siah ubiquitin ligase is structurally related to TRAF and modulates TNF-α signaling. *Nat. Struct. Biol.* **9,** 68–75
61. Metzger, M. B., Hristova, V. A., and Weissman, A. M. (2012) HECT and RING finger families of E3 ubiquitin ligases at a glance. *J. Cell Sci.* **125,** 531–537
62. Andréola, M. L. (2009) Therapeutic potential of peptide motifs against HIV-1 reverse transcriptase and integrase. *Curr. Pharm. Des.* **15,** 2508–2519
63. Huber, K. L., Ghosh, S., and Hardy, J. A. (2012) Inhibition of caspase-9 by stabilized peptides targeting the dimerization interface. *Biopolymers* **98,** 451–465
64. Lebon, F., and Ledecq, M. (2000) Approaches to the design of effective HIV-1 protease inhibitors. *Curr. Med. Chem.* **7,** 455–477
65. McMillan, K., Adler, M., Auld, D. S., Baldwin, J. J., Blasko, E., Browne, L. J., Chelsky, D., Davey, D., Dolle, R. E., Eagen, K. A., Erickson, S., Feldman, R. I., Glaser, C. B., Mallari, C., Morrissey, M. M., Ohlmeyer, M. H., Pan, G., Parkinson, J. F., Phillips, G. B., Polokoff, M. A., Sigal, N. H., Vergona, R., Whitlow, M., Young, T. A., and Devlin, J. J. (2000) Allosteric inhibitors of inducible nitric oxide synthase dimerization discovered via combinatorial chemistry. *Proc. Natl. Acad. Sci. U.S.A.* **97,** 1506–1511
66. Laskowski, R. A., Rullmannn, J. A., MacArthur, M. W., Kaptein, R., and Thornton, J. M. (1996) AQUA and PROCHECK-NMR: programs for checking the quality of protein structures solved by NMR. *J. Biomol. NMR* **8,** 477–486
67. Koradi, R., Billeter, M., and Wüthrich, K. (1996) MOLMOL: A program for display and analysis of macromolecular structures. *J. Mol. Graph.* **14,** 51–55